Mediterranean Smart Cities Conference (MSCC 2024)
2-4 May, 2024, Martil, Morocco

Design and Optimization of MIMO Antennas for WiMAX/LTE/WLAN/5G Applications in Sub-6 GHz Wireless Communications

Moussab Chbeine
Laboratory of C3S, Faculty of Sciences and Technologies
Abdelmalek Essaâdi University
Tangier, Morocco
moussab.chbeine@etu.uae.ac.ma

Yassir Zardoua
Laboratory of C3S, Faculty of Sciences and Technologies
Abdelmalek Essaâdi University
Tangier, Morocco
yassirzardoua@gmail.com

Abdelali Astito
Laboratory of C3S, Faculty of Sciences and Technologies
Abdelmalek Essaâdi University
Tangier, Morocco
abdelali_astito@yahoo.com

Abstract—**This article presents the design of MIMO antennas for sub-6 GHz frequencies in the context of 5G, based on two symmetrical circular patches mounted on an FR4 substrate with dimensions of 70x25x1.6 mm³. Meticulously arranged slots have been integrated into the antenna structure to optimize its performance. The application of the Defected Ground Structure (DGS) technique has refined the current distribution, resulting in improved performance with a notable S11 reflection coefficient (⩽-10 dB). This antenna is capable of generating resonances at 3.6 GHz and 4.6 GHz, providing frequency coverage from 3.2 to 5.8 GHz. Specifically designed to target bands n77, n78, and n79, as well as LTE bands 22/42/43/46, this innovation represents a significant advancement for applications such as WiMAX, WLAN, LTE, and sub-6 GHz 5G, reflecting the significant potential of these technologies in the evolution of wireless communication systems.**

Keywords—MIMO antenna, 5G, LTE, WLAN, Multi-Slot, Sub-6GHz.

I. INTRODUCTION

With the continuous growth of customer base and rapid advancements in the wireless communication technology sector, it is crucial to increase the throughput and capacity of transmission channels. The adoption of systems with multiple antennas in a portable device is emerging as an effective approach to enhance the quality and speed of the communication network. In this context, Multiple Input, Multiple Output (MIMO) technology plays a central role in current research, especially in the development of 5G [1]. The field of telecommunications has recently witnessed significant breakthroughs. Since the introduction of the first generation of mobile communications (1G), followed by the innovations of 2G and 3G, and the establishment of the 4G standard, the sector has consistently evolved. Currently, with several countries in the deployment phase, 5G is poised to be the next major technological advancement. For its deployment, 5G envisions the use of two primary frequency bands for wireless communication: frequencies below 6 GHz [2-9] and those corresponding to millimeter or microwave waves. The Sub-6 GHz spectrum, already utilized in existing wireless networks, is considered a preferred option by operators for the initial deployment of 5G. This preference mainly stems from its compatibility with current infrastructures that do not require major hardware changes. This spectrum includes the n77/n78/n79 bands, covering frequencies ranging from (3.3–4.2) to (3.3–3.8) and (4.4–5.0) GHz. To meet the requirements of 5G, various methods to enhance performance are currently under study and are the subject of publications in the field.

Recent studies published in specialized journals have examined different MIMO antenna configurations designed for 5G networks operating below 6 GHz [10–17]. Next-generation antennas differ from their earlier versions in terms of reduced bandwidth or increased mutual coupling. It is essential to note that reducing mutual coupling and decreasing the coefficients of coupling efficiency (ECC) between adjacent antenna elements can lead to an increase in the antenna's size. These considerations play a vital role in the design of MIMO antennas intended for portable devices [19]. Therefore, a crucial challenge in designing antennas for portable devices is integrating multiple antennas within a limited space while ensuring sufficient isolation between them. Various strategies to reduce mutual coupling between MIMO antenna elements have been documented and are proposed in specialized literature [20]. Understanding the impact of specific absorption losses on antenna performance, especially how they are affected by the user's body, is critical. It is vital to minimize mutual coupling or improve isolation between antenna elements, particularly in the context of MIMO antennas [21]. It is also important to thoroughly evaluate other performance indicators such as

Channel Capacity Loss (CCL), Diversity Gain (DG), and Total Active Reflection Coefficient (TARC) for a comprehensive performance analysis [21,22]. Microstrip antennas are often favored for their cost-effectiveness, ease of manufacturing, and straightforward installation. However, they come with certain drawbacks such as relatively low gain, limited bandwidth, reduced efficiency, and restricted power handling capability. To improve bandwidth, various techniques are employed, including adding slots to the radiators of microstrip patch antennas, impedance tuning, increasing the substrate height, and overlaying patches on the antenna ground plane [23,24].

This article presents a two-port MIMO antenna characterized by remarkable isolation and advantageous bandwidth properties. It consists of two identical circular patches symmetrically arranged on a substrate with dimensions of 70 × 25 × 1.6 mm³. The antenna exhibits resonances at 3.6 GHz and 4.6 GHz within a range of 3.2 to 5.8 GHz, making it suitable for the NR77/78/79 bands for sub-6 GHz 5G communication, as well as WiMAX, WLAN, and LTE bands 22, 42, 43, and 46. The article also examines other relevant parameters of the MIMO antenna to analyze its performance, including S-parameters, radiation patterns, efficiency, current distribution, ECC, DG, and TARC.

II. ANTENNA DESIGN AND SIMULATED RESULTS

A. *Antenna Design*

Figures 1 and 2 provide intricate details on the layout of the MIMO antenna. Specifically, figure 1a and 1b show the front and side views of a single antenna element, whereas Figures 2a and 2b offer insights into the top and back views of the complete MIMO antenna system. Each antenna element has dimensions of 25 × 25 mm² and is constructed on an FR4 substrate. This substrate is 1.6 mm thick, has a relative permittivity of 4.3, and features a loss tangent (tanδ) of 0.025. A circular radiator and a rectangular feed line, connected through a 50 Ω transmission line, are situated on the substrate's top side. The substrate's underside is equipped with a partial ground plane that includes slots designed to decrease interference. For the MIMO antenna construction, this single unit is duplicated and rotated 90 degrees around the x-axis, with a strategic separation between elements to minimize mutual interference, culminating in the antenna's total size of 70 × 25 × 1.6 mm³.

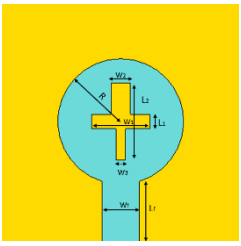

(a)

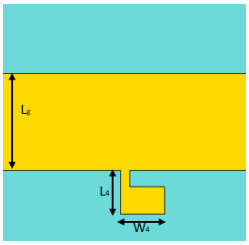

(b)

Figure 1. Geometrical specification of the unit element of MIMO antenna (a) front view, (b) back view.

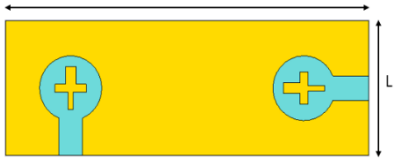

(a)

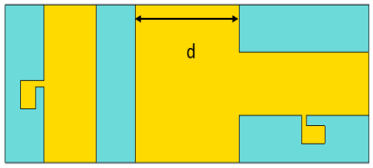

(b)

Figure 2. Geometrical specification of the MIMO antenna, (a) front view, (b) back view.

TABLE I. OPTIMIZED DESIGN PARAMETERS OF THE PROPOSED ANTENNA.

Parameter	Dimension (mm)
W_s	70
L_s	25
W_1	6
L_1	1.5
W_2	1.8
L_2	8
W3	1.8
L_g	10
W_4	5.8
L_4	3.2
W_f	3.1
L_f	12.5
R	6.5
d	20

B. *Analysis of the single antenna and stages in the evolution of antenna design*

Evolution in Antenna Design: This section explores the various stages of development of the single antenna element in question. Three distinct phases (from Stage 1 to

Stage 4) are detailed, accompanied by a comparative analysis based on |S11| (dB) measurements illustrated in Figure 3. Initially, Stage 1 involved a circular radiator with a simple ground plane. In the second stage, although slots were added to the radiator to create a configuration similar to the symbol "+," the results obtained in the sub-6 GHz frequency band were unsatisfactory. At the third stage, the introduction of a partial ground plane greatly altered the operational frequency band, yet did not achieve the desired results. A significant breakthrough was achieved with the fourth iteration of the antenna, building upon the foundations of the third stage while incorporating specific adjustments to its rear structure. The precise incorporation of slots in this partial ground plane resulted in marked improvements, substantially influencing the antenna's resonance characteristics. This translated into a significant enhancement in performance, aligning with the targeted frequencies. The comparative examination of these different configurations highlights the intricacy and complexity involved in designing antennas suitable for sub-6 GHz applications, confirming the significance of every adjustment, even minor ones, on the overall antenna performance.

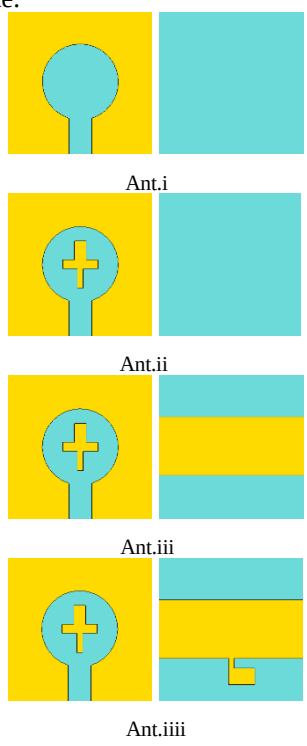

Figure 3. Antenna Design Evolution.

The simulation results for the reflection coefficient are illustrated in Figure 4, displaying the evolution of the antenna across four stages.

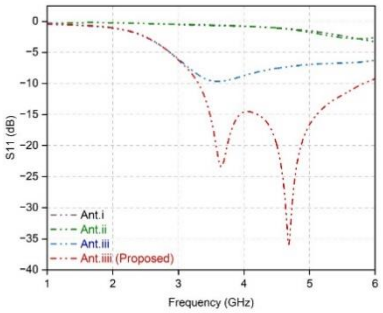

Figure 4. Simulated Response of Reflection Coefficients in Design Stages.

C. *Parametric Study*

The analysis of the S-parameter responses of the examined antenna was conducted through detailed parametric studies, as shown in Figure 4. These studies highlight the impact of slight variations in various antenna parameters on the S-parameter response. For the sake of brevity, we will focus on two parameters, namely R and W4. Figure 4 demonstrates how changing the radius length R influences the reflection coefficient. By adjusting R in 1 mm increments, significant changes in operating frequency and the reflection coefficient were observed, as illustrated in the figure below.

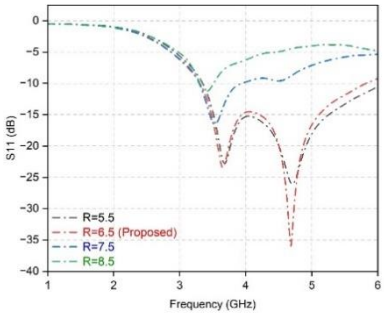

Figure 5. Parametric Analysis with Respect to R

Regarding Figure 5, it highlights the impact of varying the width W4. An increase in W4 results in a shift of resonance towards higher frequencies and alters the reflection coefficient, indicating impedance matching. Just like R, W4 plays a crucial role in the resonance behavior of the antenna, influencing the resonance frequency as shown in the figure below.

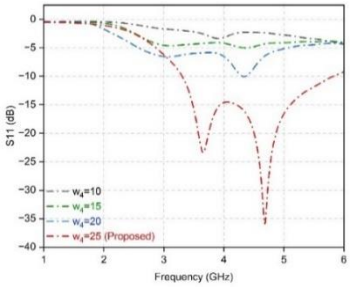

Figure 6. Parametric Analysis with Respect to W4

III. DIVERSITY PERFORMANCES

A. *Reflection Coefficient Results*

Figure 6 presents the simulated results of the reflection coefficient for the MIMO antenna. From Figure 3, it is clearly observable that the simulation results align with expectations. The circular patch antenna manages to generate resonances at 3.6 GHz and 4.6 GHz, with an S11 reflection coefficient of at least -10 dB. This results in a 10 dB bandwidth of 2600 MHz (from 3.6 to 5.8 GHz), allowing coverage of sub-6 GHz 5G-NR bands such as n48, n77, n78, and n79.

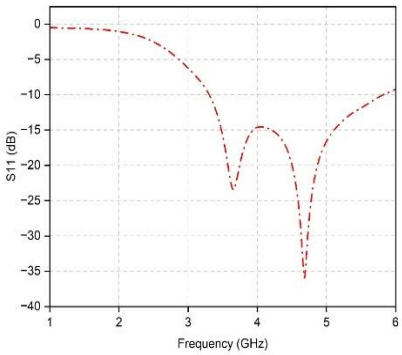

Figure 7. Simulated Reflection Coefficient

B. *Gain and Radiation Patterns*

Gain is a parameter utilized for assessing the effectiveness of the suggested MIMO antenna configuration. Simulations indicate that the proposed MIMO antenna exhibits a gain of approximately 2.42 dBi at 3.6 GHz and 2.69 dBi at 4.6 GHz, as shown in Figure 7.

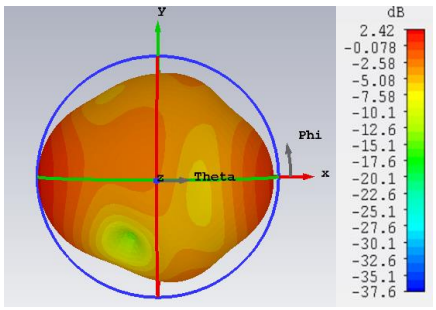

(a)

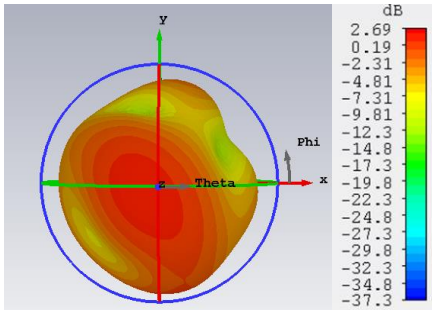

(b)

Figure 8. Simulated 3D radiation patterns at (a) 3.6 GHz and (b) 4.6 GHz

The 2D radiation patterns for the suggested antenna at two different frequencies are depicted in Figures 8(a) and 8(b), showcasing the E and H planes at 3.6 GHz and 4.6 GHz, respectively. The antenna demonstrates a dipole-like radiation behavior at its resonance frequencies. This characteristic pattern is attributed to the unique design feature of dual circular rings on the patch, combined with a partially segmented ground plane.

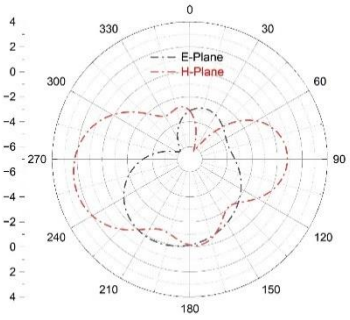

(a)

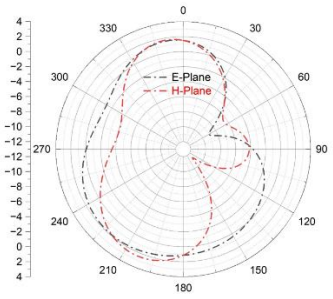

(b)

Figure 9. Simulated radiation patterns at (a) 3.6 GHz and (b) 4.6 GHz in the principal planes E-plane and H-plane.

Figure 9 depicts the overall simulated realized gain for the proposed antenna, which attained a peak realized gain of 3.36 dBi throughout the entire target bandwidth.

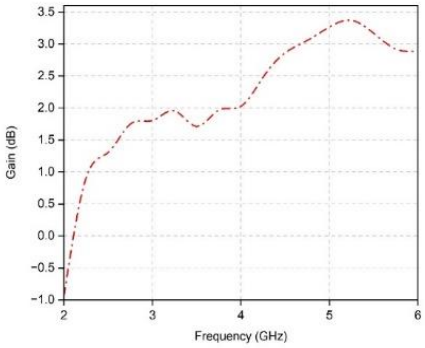

Figure 10. Gain of the Proposed Antenna.

C. *EFFICIENCY*

Figure 10 demonstrates the frequency-dependent efficiency of the suggested MIMO antenna design. Throughout the entire intended bandwidth, this antenna design maintains high efficiency, peaking at a value of 94%.

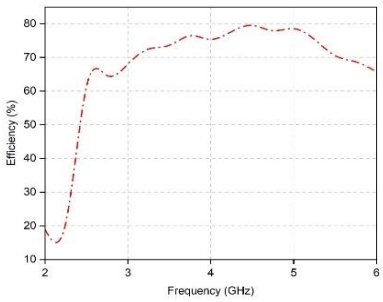

Figure 11. Efficiency of the Proposed Antenna.

D. Surface Current Distribution

The surface current distribution on the proposed MIMO antenna at two different frequencies, namely 3.6 GHz and 4.6 GHz, is illustrated in Figure 11. This representation is obtained with port 1 activated, while the other port is terminated with a 50-ohm impedance to prevent current from propagating to the neighboring antenna element, thus reducing mutual coupling. It highlights that the current density is primarily concentrated around the feedline. Peak current densities are measured at 63.7 A/m at 3.6 GHz and 52.1 A/m at 4.6 GHz for the respective bands.

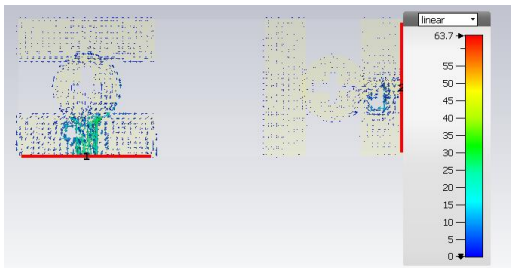

(a)

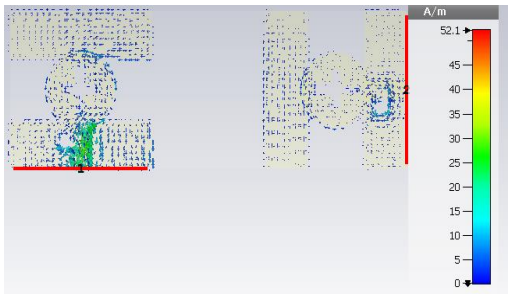

(b)

Figure 12. MIMO antenna surface current distribution from port 1 at: (a) 3.6 GHz and (b) 4.6 GHz

E. Envelope Correlation Coefficient And Diversity Gain

ECC is a key factor for measuring the intra-element isolation (degree of signal fading) between the four-port MIMO antenna. This parameter must be less than 0.5 for good diversity gain[25]. To obtain more realistic results, the ECC was calculated from 3D radiation pattern according to equation (1).

$$ECC(i,j) = \frac{\left(\oint\left(X_{PR}E_{\theta i}(\Omega)E^{*}{}_{\theta j}(\Omega)P_{\theta}(\Omega)+E_{\phi i}(\Omega)E^{*}{}_{\phi j}(\Omega)P_{\phi}(\Omega)\right)d(\Omega)\right)^{2}}{\oint\left(X_{PR}G_{\theta i}(\Omega)P_{\theta}(\Omega)+G_{\phi i}(\Omega)P_{\phi}(\Omega)\right)d(\Omega).\oint\left(X_{PR}G_{\theta j}(\Omega)P_{\theta}(\Omega)+G_{\phi j}(\Omega)P_{\phi}(\Omega)\right)d(\Omega)} \quad (1)$$

In the provided context, X_{PR} is defined as the cross-polarization power ratio within the propagation environment. This metric is integral to the preceding formula.,$G_{\theta}(\Omega) = E_{\theta}(\Omega)E^{*}{}_{\theta}(\Omega)$ and$G_{\phi}(\Omega) = E_{\phi}(\Omega)E^{*}{}_{\phi}(\Omega)$ These refer to the power patterns for θ and ϕ polarizations, respectively. $P_{\theta}(\Omega)$ and$P_{\phi}(\Omega)$represent the angular density functions of the θ and ϕ polarizations, respectively.

$E_{\theta i}(\Omega)$ and $E_{\theta j}(\Omega)$ are the electric field patterns of the ith and jth antenna elements in the θ polarization, respectively. $E_{\phi i}(\Omega)$and$E_{\phi j}(\Omega)$ are the electric field patterns of the ith and jth antenna elements in the φ polarization, respectively[26].

For a lossless MIMO system, the ECC calculated from the S parameters according to the following equation (2).

$$ECC = \frac{\left|\sum_{n=1}^{N} S_{i,n}^{*} S_{n,j}\right|^{2}}{\prod_{k=i,j}\left[1-\left|\sum_{n=1}^{N} S_{i,n}^{*} S_{n,k}\right|\right]} \quad (2)$$

Where: ECC denotes the envelope correlation coefficient; i and j are the number of ports.

The diversity gain in a MIMO system is employed to determine an overall increase in signal-to-noise ratio (SNR) by utilizing certain diversity combining techniques such as maximal ratio combining (MRC) [27], equal-gain combining (EQ) and selection combining (SC). The DG is mainly dependent on a large part of the ECC , as shown in the following equation (3) [28].

$$DG = 10\sqrt{(1-|\rho|^{2})} \quad (3)$$

Where ρ is the complex cross correlation coefficient, and $|\rho|^{2} = ECC$

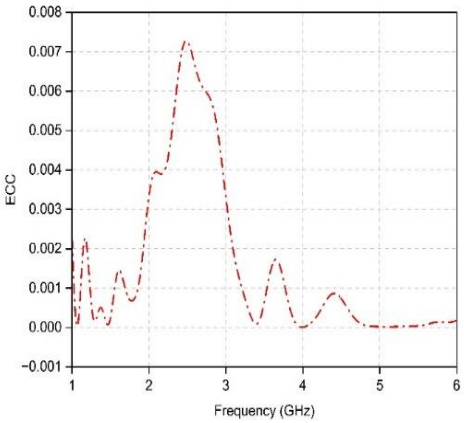

Figure 13. Envelope correlation coefficient curve from S parameters

The ECC (Antenna Correlation Coefficient) and DG (Diversity Gain) coefficients for the MIMO system, derived from the S-parameters, are presented in Figures 12 and 13. As shown in Figure 12, the calculated ECC is less than 0.007, indicating low correlation between the antennas. Additionally, Figure 13 illustrates the system's

diversity gain, which proves to be greater than 9.96 dB, covering the entire operational bandwidth of the antenna.

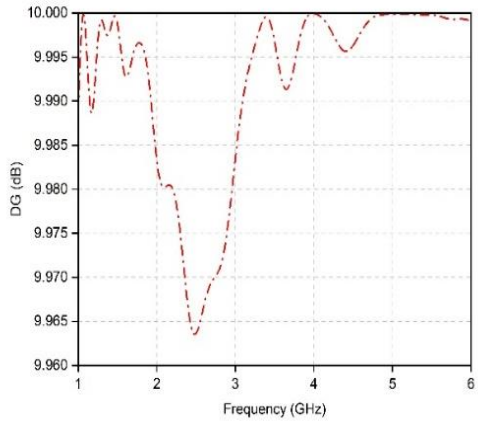

Figure 14. Diversity gain curve from S parameters

F. Total Active Reflection Coefficient

Evaluating the total active reflection coefficient is essential for the effective performance of MIMO antennas. This coefficient can be ascertained through the application of S-parameters. Specifically, for a MIMO antenna with two ports, the TARC is characterized in the following manner [29, 30]:

$$TARC = \sqrt{\frac{|S_{11}+S_{12}e^{j\theta}|^2+|S_{21}+S_{22}e^{j\theta}|^2}{2}} \qquad (4)$$

According to Figure 14, it is observed that the value of the Total Active Reflection Coefficient (TARC) for the designed MIMO antenna is below -10 dB. This measurement thus meets the performance requirements for MIMO systems.

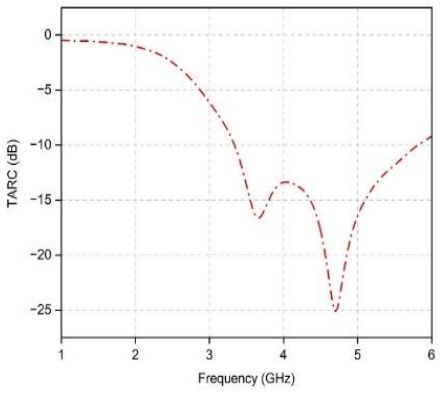

Figure 15. Simulated TARC of the proposed MIMO antenna

IV. PERFORMANCE COMPARISON

TABLE II. PERFORMANCE COMPARISON WITH PREVIOUS PUBLISHED LITERATURE

Ref. No.	Size in term of (mm2)	Oper. Bands (GHz)	Isol. (dB)	Div. gain	ECC
Proposed	70×25	3.6-5.8	>17.4	>9.964	<0.007
[31]	122 × 110	0.5–3.0	>15.5	>9.962	<0.085
[32]	105 × 125	2.3–2.9	>15	>9.983	<0.15
[33]	95 × 60	1.0–3.0	>16	>9.987	<0.089
[34]	110 × 114	2.0–6.0	>20	>9.476	-
[35]	60 × 60	2.3–2.4	>31	>9.947	<0.26
[36]	30 × 65	2.0–6.0	>28	>9.953	<0.1
[37]	94 × 94	1.1–1.7	>14	>9.974	<0.07

V. CONCLUSION

This study introduces a novel MIMO antenna configuration tailored for LTE and sub-6 GHz 5G frequencies. The design features two overlapping circular radiators with incorporated slots and a split ground plane, all mounted on an FR4 substrate measuring 70x25x1.6 mm³. This antenna supports a broad frequency range from 3.2 to 5.8 GHz, covering all sub-6 GHz 5G frequencies, in addition to WiFi, WLAN, and LTE bands 22, 42, 43, and 46. Furthermore, the antenna exhibits remarkable diversity performance, with low ECC (< 0.007), high DG (≥ 9.964), and TARC (≤ -10 dB).

ACKNOWLEDGMENT

This work was partially supported by the Information Systems and Telecommunications Laboratory at Abdelmalek Essaadi University, Tetuan, Morocco

REFERENCES

[1] Hua, Q. *et al.* A "dual-band dual-polarized base station antenna using a novel feeding structure for 5G communications," *IEEE Access* 8, 63710–63717 (2020).

[2] Alibakhshikenari, M. *et al.* A comprehensive survey of "metamaterial transmission-line based antennas: Design, challenges, and applications," *IEEE Access* 8, 144778–144808 (2020).

[3] Alibakhshikenari, M. *et al.* "Beam-scanning leaky-wave antenna based on CRLH-metamaterial for millimetre-wave applications.*IET Microwav. Antennas Propag*," 13, 1129–1133 (2019).

[4] Alibakhshikenari, M., Virdee, B. S., Ali, A. & Limiti, E. A "novel monofilar-Archimedean metamaterial inspired leaky-wave antenna for scanning application for passive radar systems. *Microw*," *Opt. Technol. Lett.* 60, 2055–2060 (2018).

[5] Alibakhshikenari, M. *et al.* "Bandwidth and gain enhancement of composite right left-handed metamaterial transmission line planar antenna employing a non-foster impedance matching circuit board," *Sci. Rep.* 11, 7472 (2021).

[6] Alibakhshikenari, M. *et al.* " An innovative antenna array with high inter element isolation for sub-6 GHz 5G MIMO communication systems," *Sci. Rep.* 12, 7907 (2022).

[7] Alibakhshikenari, M. *et al.* "A comprehensive survey on antennas on-chip based on metamaterial, metasurface, and substrate integrated waveguide principles for millimeter-waves and terahertz integrated circuits and systems," *IEEE Access* 10, 3668–3692 (2022).

[8] Alibakhshikenari, M. *et al.* "Dual-polarized highly folded bowtie antenna with slotted self-grounded structure for sub-6 GHz 5G applications," *IEEE Trans. Antennas Propag.* 70, 3028–3033 (2022).

[9] Fakharian, M. M., Alibakhshikenari, M., See, C. H. & Abd-Alhameed, R. "A high gain multiband offset MIMO antenna based on a planar log-periodic array for Ku/K-band applications," *Sci. Rep.* 12, 4044 (2022).

[10] Ban, Y.-L., Li, C., Sim, C.-Y.-D., Wu, G. & Wong, K.-L. “4G/5G multiple antennas for future multi-mode smartphone applications,”.*IEEE Access* 4, 2981–2988 (2016).
[11] Guo, J., Cui, L., Li, C. & Sun, B. “ Side-edge frame printed eight-port dual-band antenna array for 5G smartphone applications,” *IEEE Trans. Antennas Propag.* 66, 7412–7417 (2018).
[12] Han, C.-Z., Xiao, L., Chen, Z. & Yuan, T. “Co-located self-neutralized handset antenna pairs with complementary radiation patterns for 5G MIMO applications,” *IEEE Access* 8, 73151–73163 (2020).
[13] Hu, W. *et al.* “Dual-band ten-element MIMO array based on dual-mode IFAs for 5G terminal applications,” *IEEE Access* **7**, 178476–178485 (2019).
[14] Dwivedi, A. K., Sharma, A., Pandey, A. K. & Singh, V. “Two port circularly polarized MIMO antenna design and investigation for 5G communication systems,”*Wirel. Pers. Commun.* 120, 2085–2099 (2021).
[15] Ren, Z. & Zhao, A. “Dual-band MIMO antenna with compact self-decoupled antenna pairs for 5G mobile applications,” *IEEE Access* **7**, 82288–82296 (2019).
[16] Sun, L., Feng, H., Li, Y. & Zhang, Z. “Compact 5G MIMO mobile phone antennas with tightly arranged orthogonal-mode pairs,” *IEEE Trans. Antennas Propag.* 66, 6364–6369 (2018).
[17] Wang, H., Zhang, R., Luo, Y. & Yang, G. “ Compact eight-element antenna array for triple-band MIMO operation in 5G mobile terminals,”*IEEE Access* 8, 19433–19449 (2020).
[18] Zhao, A. & Ren, Z. “Size reduction of self-isolated MIMO antenna system for 5G mobile phone applications,”*IEEE Antennas Wirel.Propag. Lett.* 18, 152–156 (2019).
[19] Singh, A. K. *et al.* “ A compact MIMO antenna for 5G NR frequency communication,” *IETE J. Res.*(2022).
[20] Abbas, A. *et al.* “ Highly selective multiple-notched UWB-MIMO antenna with low correlation using an innovative parasitic decoupling structure,”*Eng. Sci. Technol. Int. J.* 43, 101440 (2023).
[21] Kiani, S.H.; Altaf, A.; Abdullah, M.; Muhammad, F.; Shoaib, N.; Anjum, M.R.; Damaševi˘cius, R.; Blažauskas, T. “Eight Element Side Edged Framed MIMO Antenna Array for Future 5G Smart Phones,” *Micromachines* 2020, *11*, 956.
[22] Abdullah, M.; Altaf, A.; Anjum, M.R.; Arain, Z.A.; Jamali, A.A.; Alibakhshikenari, M.; Falcone, F.; Limiti, E. “Future Smartphone: MIMO Antenna System for 5G Mobile Terminals,” *IEEE Access* 2021, *9*, 91593–91603.
[23] Mao, C.-X.; Khalily, M.; Xiao, P.; Brown, T.W.C.; Gao, S. “Planar Sub-Millimeter-Wave Array Antenna with Enhanced Gain and Reduced Sidelobes for 5G Broadcast Applications,”*IEEE Trans. Antennas Propag.* 2019, *67*, 160–168.
[24] Ali, I.; Jamaluddin, M.H.; Gaya, A.; Rahim, H.A. “A Dielectric Resonator Antenna with Enhanced Gain and Bandwidth for 5G Applications,” *Sensors* 2020, *20*, 675.
[25] L. Malviya, R. K. Panigrahi, and M. V. Kartikeyan, “MIMO antennas with diversity and mutual coupling reduction techniques: A review,” Int. J. Microw. Wirel. Technol., vol. 9, no. 8, pp. 1763–1780, 2017.
[26] Z. Ren and A. Zhao, “Dual-Band MIMO Antenna with Compact SelfDecoupled Antenna Pairs for 5G Mobile Applications,” IEEE Access, vol. 7, pp. 82288–82296, 2019.
[27] F. Wang, Z. Duan, X. Wang, Q. Zhou, and Y. Gong, “High isolation millimeter-wave wideband MIMO antenna for 5G communication,”Int. J. Antennas Propag., vol. 2019, pp. 1–12, 2019
[28] A. K. Sohi and A. Kaur, “UWB aperture coupled circular fractal MIMO antenna with a complementary rectangular spiral defected ground structure (DGS) for 4G/WLAN/radar/satellite/international space station (ISS) communication systems,” J. Electromagn. Waves Appl., vol. 34, no. 17, pp. 2317–2338, (2020), doi: 10.1080/09205071.2020. 1813638.x
[29] Chae, S., S. Oh, and S. Park, “Analysis of mutual coupling, correlations,and TARC in WiBro MIMO array antenna," IEEE Antennas and Wireless Propagation Letters, Vol. 6, 122-125, 2007.
[30] Fritz-Andrade, E., H. Jardon-Aguilar, and J. A. Tirado-Mendez, “The correct application of total active reflection coefficient to evaluate MIMO antenna systems and its generalization to N ports,"Int. J. RF Microw. Comput. Eng., Vol. 30, No. 4, 1-10, 2020.
[31] Morsy MM, Morsy AM. “Dual-band meander-line MIMO antenna with high diversity for LTE/UMTS router,” IET Microwaves Antennas Propag 2017;12(3):395–9.
[32] Moradikordalivand A, et al. “Wideband MIMO antenna system with dual polarization for WiFi and LTE applications,” Int J Microwave Wireless Technolog 2016;8(3):643.
[33] Ding Y, et al. “A novel dual-band printed diversity antenna for mobile terminals,” IEEE Trans Antennas Propag 2007;55(7):2088–96.
[34] Lin S-Y, Huang H-R. “Ultra-wideband MIMO antenna with enhanced isolation,” Microwave Opt Technol Lett 2009;51(2):570–3.
[35] Jiang T, Jiao T, Li Y. “ A Low Mutual Coupling MIMO Antenna Using Periodic MultiLayered Electromagnetic Band Gap Structures,” Appl Comput Electromagnet Soc J 2018; 33:3.
[36] Cui S, et al. “Compact dual-band monopole antennas with high port isolation,” Electron Lett 2011 ;47(10) :579–80.
[37] Yao Y, et al. “ Novel diversity/MIMO PIFA antenna with broadband circular polarization for multimode satellite navigation,” IEEE Antennas Wirel Propag Lett 2012; 11:65–8.